Bridging Hydroxyls on Anatase TiO_2 (101) by Water Dissociation in Oxygen Vacancies

Immad M Nadeem, George T Harrison, Axel Wilson, Chi L Pang, Jörg Zegenhagen, Geoff Thornton

THE JOURNAL OF PHYSICAL CHEMISTRY B

Article

pubs.acs.org/JPCB

Bridging Hydroxyls on Anatase TiO_2(101) by Water Dissociation in Oxygen Vacancies

Immad M. Nadeem,[†,‡] George T. Harrison,[†] Axel Wilson,[†] Chi L. Pang,[†] Jörg Zegenhagen,[‡] and Geoff Thornton*[,†]

[†]London Centre for Nanotechnology and Department of Chemistry, University College London, 20 Gordon Street, London, WC1H 0AJ, U.K.

[‡]Diamond Light Source Ltd., Harwell Science and Innovation Campus, Didcot, Oxfordshire, OX11 0DE, U.K.

ABSTRACT: Titanium dioxide is a promising candidate for photocatalytic H_2 fuel production, and understanding water splitting on TiO_2 surfaces is vital toward explaining and improving the generation of H_2. In this work, we electron irradiate anatase TiO_2(101) at room temperature to create metastable surface oxygen vacancies in order to investigate their ability to dissociate H_2O. Our scanning tunneling microscopy investigations suggest that the surface oxygen vacancies can dissociate H_2O by forming bridging OH species. This claim is supported by theoretical calculations from the literature and our previously published spectroscopic measurements.

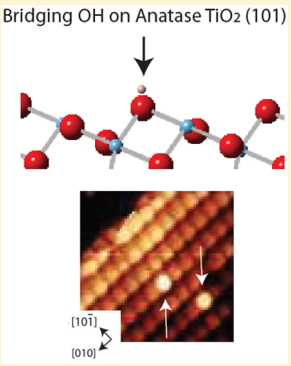

1. INTRODUCTION

Light harvesting metal oxides photocatalytically split water to produce H_2 fuel.[1] Since Honda and Fujishima[2] showed the potential of TiO_2 in this respect, it has been widely studied.[3−6] TiO_2 is a low cost, highly photostable, and nontoxic material that displays high catalytic efficiency.[7] Three polymorphs of TiO_2 exist in nature: rutile, anatase, and brookite.[8] Anatase and rutile are the most active and studied polymorphs with research extending from engineering materials[3−6] to fundamental work.[9−13] *Rutile TiO_2(110)* (R_{110}) and *anatase TiO_2(101)* (A_{101}) are the most stable faces of the respective polymorphs. The former has been the focus of numerous publications,[9−11] whereas research on the latter is less well documented.

A_{101} consists of 5 (Ti_{5c}) and 6 (Ti_{6c}) coordinate Ti and 2 (O_{2c}) and 3 (O_{3c}) coordinate O in a sawtooth-like geometry[14,15] (see Figure 1). In principle, the surface can maintain *bridging OH* (OH_{br}) (i.e., H adatom on O_{2c}) and *terminal OH* (OH_t) (i.e., OH adsorbed to Ti_{5c}). Scanning tunneling microscopy (STM) images of A_{101} show trapezoidal terraces and sphere-like features that represent a Ti_{5c}−O_{2c} pair[14] (see Figure 2). Electron irradiation of A_{101} creates *surface O_{2c} vacancies* (V_o) that are unstable above 200 K and migrate to the subsurface and bulk.[16−18]

The temperature and pressure dependence of H_2O adsorption on A_{101} has been examined.[18−23] In ultrahigh vacuum (UHV), there is little or no evidence of H_2O adsorption at room temperature, although adsorption is increasingly favored below 298 K.[20] In UHV at 6 K, STM tip pulsing (a voltage pulse applied to the surface via the STM tip) can transform H_2O into features thought to be OH_t.[22] Co-dosing O_2 and H_2O on A_{101} at 105 K and subsequently annealing for 10 min at room temperature, followed by STM (at 6 K), also yields features thought to be OH_t.[18] In UHV at 120 K, water has been adsorbed on A_{101} with photoemission measurements collected at intervals from 160 to 400 K. The results indicate that water adsorbs in a mixed associative and dissociative state below 300 K.[21] At room temperature, photoemission measurements of A_{101} under exposure to water pressures of 0.6−6 mbar indicate mixed associative and dissociative adsorption of water.[23] In UHV, at 100 K and under UV illumination, H_2O adsorbed on A_{101} has been observed to generate gaseous OH species. This has been interpreted as the adsorbed H_2O dissociating into OH_{br} and OH_t where the latter leaves the surface.[24] As for theory, first-principles molecular dynamics calculations predict that H_2O can dissociate in V_o[25,26] and that the A_{101} and liquid water interface (at 300−400 K) can maintain OH_t and OH_{br} species.[27,28]

In the literature, scanning probe microscopy (SPM) of OH_t[18,22] on A_{101} is reported, while SPM of OH_{br}[29] is relatively briefly discussed. Similar to A_{101}, R_{110} consists of Ti_{5c}, Ti_{6c}, O_{2c}, and O_{3c} species, with the two surfaces differing in their bond angles.[9−11] OH_{br} can form on R_{110} via dissociation of H_2O from the residual vacuum at V_o sites.[9,10] In previous work,[30] we presented spectroscopic evidence of OH formation on the A_{101} surface via H_2O dissociation in V_o. In this paper, we describe an STM study that identifies the OH species as OH_{br}.

Special Issue: Miquel B. Salmeron Festschrift

Received: July 14, 2017
Revised: September 12, 2017

DOI: 10.1021/acs.jpcb.7b06955
J. Phys. Chem. B XXXX, XXX, XXX−XXX

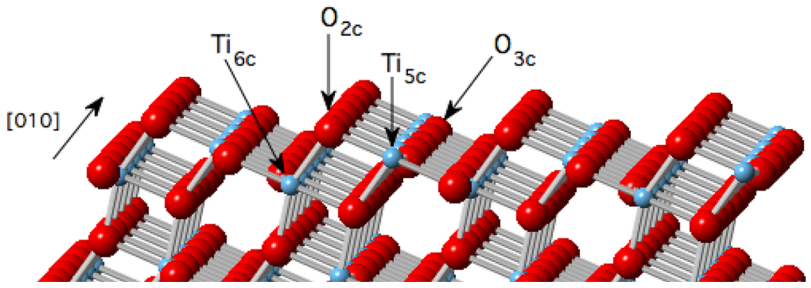

Figure 1. Illustration of the A_{101} surface with the Ti_{5c}, Ti_{6c}, O_{3c}, and O_{2c} labeled.

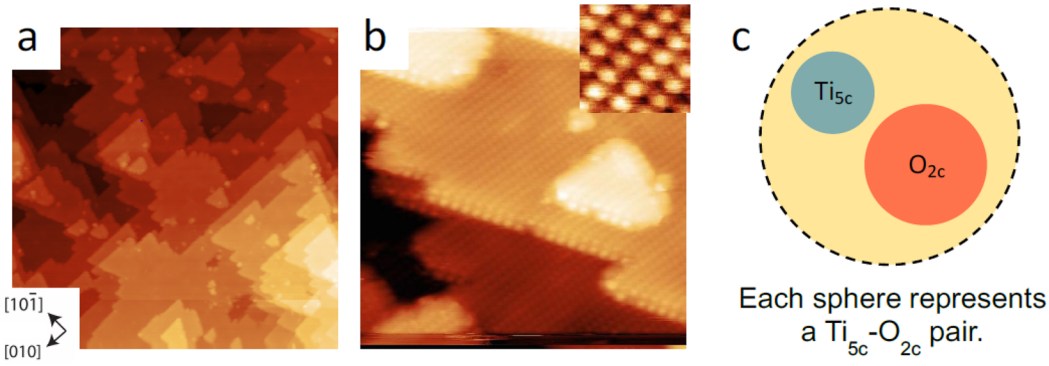

Figure 2. (a) 100 × 100 nm^2 STM image of A_{101} (V_s = +1.6 V, I_t = 0.4 nA). (b) 15 × 15 nm^2 STM image of A_{101} (V_s = +1.1 V, I_t = 0.6 nA) with the inset (2 × 2 nm^2) illustrating the sphere-like features observed with STM. (c) Illustration that each sphere-like feature in STM represents a Ti_{5c}–O_{2c} pair.

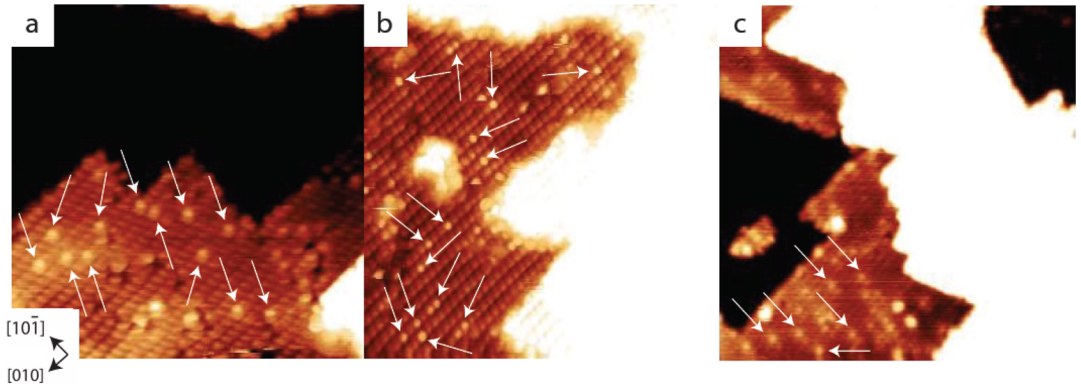

Figure 3. (a) 13 × 13 nm^2 STM image (V_s = +1.6 V, I_t = 0.5 nA) of A_{101} after electron irradiation at 500 eV, for 30 s and at a density of 37 $\mu A.cm^{-2}$. (b) 15 × 15 nm^2 STM image (V_s = +1.03 V, I_t = 0.3 nA) of A_{101} after electron irradiation at 500 eV, for 60 s and at a density of 37 $\mu A.cm^{-2}$. (c) 23 × 23 nm^2 STM image (V_s = +1.5 V, I_t = 0.4 nA) of A_{101} after electron irradiation at 50 eV, for 30 s and at a density of 74 $\mu A.cm^{-2}$.

2. EXPERIMENTAL SECTION

A natural A_{101} single crystal (3 × 3 × 1 mm^3) was purchased from *Pi Kem* and was mounted onto a Ta plate with Ta strips. The sample was prepared in UHV with cycles of Ar^+ sputtering ($P_{Ar} = 5 \times 10^{-5}$ mbar, 1 kV, 10 $\mu A.cm^{-2}$, 20 min) and annealing (T < 1023 K, 10 min).[31] Low energy electron diffraction (LEED) and Auger electron spectroscopy (AES) were used to ensure an ordered and contaminant free surface (below the detection limits of AES) for STM measurements. The STM used is an *Omicron* UHV AFM/STM instrument operated in constant current mode at room temperature using electrochemically etched tungsten tips, which were degassed in UHV and conditioned during scanning with voltage pulses of up to 10 V. All STM imaging was carried out by tunneling into empty states using positive sample bias voltages in the range from 1 to 1.6 V. The base pressure of the instrument was 5×10^{-10} mbar.

An outgassed filament was used for electron irradiation, with a negative bias with respect to the grounded sample. The front face of the sample was approximately 2 cm from the filament, and the drain current from the sample was used to monitor the electron flux. During irradiation, the UHV chamber pressure increased up to the low 10^{-8} mbar range with a H_2O partial pressure up to the low 10^{-9} mbar region. Immediately after irradiation, the pressure returned to the 10^{-10} mbar region. The irradiation stimulated chamber pressure rise is largely attributed to residual UHV gases—H_2, H_2O, CO, and CO_2. At room temperature, H_2O has been experimentally shown to react with V_o to form an OH_{br} defect site on A_{101}[30] and R_{110}.[9,10] However, at room temperature, there is no evidence to suggest that either CO or CO_2 react with V_o on A_{101}[30] or R_{110}.[9,10] Therefore, the effect of H_2O on V_o can be investigated in the presence of CO and CO_2. During irradiation, the sample is expected to be

DOI: 10.1021/acs.jpcb.7b06955
J. Phys. Chem. B XXXX, XXX, XXX−XXX

mildly heated by electrons emitted from the filament. It takes at least 15 min to transfer the sample from the electron irradiation position to the STM and achieve tunneling conditions. STM presented little or no thermal drift, suggesting that the sample had returned to or was very close to room temperature. This indicates a mild increase in temperature during electron irradiation. The reactivity of the V_o created by electron-irradiation with residual H_2O in UHV (i.e., at the base pressure and during electron irradiation) was investigated with STM. We define a monolayer (ML) as corresponding to the number of surface Ti_{5c}–O_{2c} pairs (density: 5.17 nm^{-2}). ML coverages are given as averaged values ± two standard deviations.

3. RESULTS AND DISCUSSION

Figure 3 shows the A_{101} surface after three electron irradiation events. Images of the electron irradiated surface contain a number of bright features (marked with white arrows in Figure 3) that we identify as OH_{br} groups formed via H_2O dissociation in V_o. The density of bright features in Figure 3 is reported in Table 1 and is approximately 0.05 ML, independent of the electron irradiation conditions. Theory and experiment suggest that A_{101} surface defects act as excess electron "traps", where the excess electrons are loosely bound to the defect.[27,30,32] In particular, OH_{br} species on A_{101} are predicted to maintain trapped charge at the Ti_{5c} site adjacent to the OH_{br}.[27] Our previously published two-photon photoelectron (2PPE) spectroscopy and UV photoelectron spectroscopy (UPS) work[30] shows that electron irradiated A_{101} can maintain excess electrons beyond thermally equilibrated levels on the surface as OH species. While these earlier results indirectly support the electron irradiation induced formation of OH_{br} (via H_2O reacting with the V_o), STM allows us to image the position of the OH species. A high-resolution image of part of the surface imaged in Figure 3b is shown in Figure 4. The positioning of the bright feature is above the sphere-like feature of the as-prepared surface. This is consistent with the formation of OH_{br} with H bound to the O_{2c}. On A_{101}, OH_t[18,22] appear as dimer-like features. Additionally, the appearance of the bright features is reminiscent of OH_{br} observed on R_{110}.[9,10] This suggests that the bright features are surface OH_{br} on A_{101} formed via the dissociation of H_2O in a V_o.

Theory predicts that H_2O dissociation in V_o on A_{101} forms a pair of adjacent OH_{br}.[25,26] On R_{110}, this type of behavior is observed experimentally, with OH_{br} forming in adjacent pairs.[9,10] The OH_{br} subsequently diffuse (i.e., H adatom diffusion) in the [001] and [1$\bar{1}$0] direction through thermally activated pathways, where diffusion in the latter direction can be promoted by H_2O.[33,34] Our STM results for A_{101} show that the OH related bright features are largely immobile on the surface. Hence, the bright features should exist as adjacent pairs representing two OH_{br}. In contrast, the data in Figure 3 show that the bright features are well dispersed. This discrepancy could arise from thermally activated OH_{br} migration caused by heating from the filament during electron irradiation or could be due to H_2O induced mobility when the H_2O partial pressure increases during electron irradiation.[33,34] An alternative perspective could be that the bright features are not paired as, during electron irradiation, OH_{br} are being formed and desorbed simultaneously—as is the case on R_{110}.[35] Additionally, there may be a complex series of steps where paired OH_{br} initially move quickly away from each other and subsequently over time this movement could slow down and stop after the species are spread over the surface in the most energetically favorable distribution.

On R_{110}, the H adatom (associated with OH_{br} species) can be removed (pulsed off) with approximately +3 V STM tip pulses.[9,10,36] On A_{101}, STM tip pulsing (in the range +2.7 to +3.5 V) has been reported to convert OH_t to O_2.[18,22] However, the bright features under discussion do not pulse off or convert with +3 to +4 V pulses, suggesting that OH_{br} species on A_{101} are energetically more stable than those on R_{110}. This could result in less mobility and greater resistance to STM tip pulsing. Although R_{110} and A_{101} can maintain defects/adsorbates at similar sites, the behavior of these species has been shown to be different; e.g., at room temperature, V_o can exist on the R_{110} surface, whereas, on A_{101}, V_o migrates toward the bulk.[16,36] Hence, it is reasonable to suggest that other defects (such as OH_{br}) also exhibit different characteristics. Therefore, on R_{110}, pulsing can remove OH_{br}, whereas this would not necessarily be the case with A_{101}. STM tip pulsing beyond +4 V resulted in a "tip-change" which prevented high-resolution, atomically resolved STM images from being recorded.

To further probe the origin of the bright features created by electron irradiation, the surface imaged in Figure 3a was subjected to progressive electron irradiation without surface repreparation (see Figure 5 and Table 2). Each successive electron irradiation condition consists of an increase in the density of electrons irradiating the surface, whereas the electron energy and duration of irradiation were fixed at 500 eV and 30 s, respectively. As is shown in Table 2, this resulted in an increase in bright feature density as the electron density was increased. This likely arises from an increase in the density of electrons irradiating the surface that would increase the number of V_o being created and subsequently result in more H_2O molecules quenching them to form OH_{br}. Another point of

Table 1. Surface ML Coverages of the Electron Irradiated A_{101} Presented in Figure 3

electron energy (eV)	current density ($\mu A.cm^{-2}$)	duration (s)	ML coverage
500	37	30	0.05 ± 0.01
500	37	60	0.05 ± 0.01
50	74	30	0.04 ± 0.01

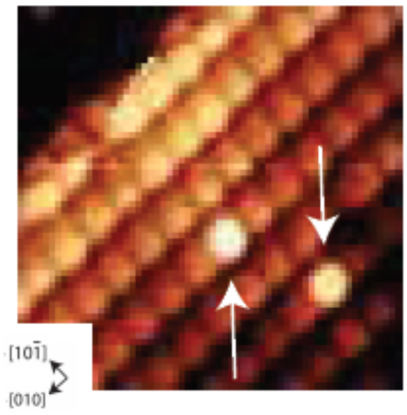

Figure 4. 3.5 × 3.5 nm^2 STM image (V_s = +1.2 V, I_t = 0.4 nA) of the A_{101} surface after electron irradiation conditions given for Figure 3b. STM image showing that the bright feature exists above the sphere-like feature on A_{101} where each sphere-like feature represents a surface Ti_{5c}–O_{2c} pair.

DOI: 10.1021/acs.jpcb.7b06955
J. Phys. Chem. B XXXX, XXX, XXX–XXX

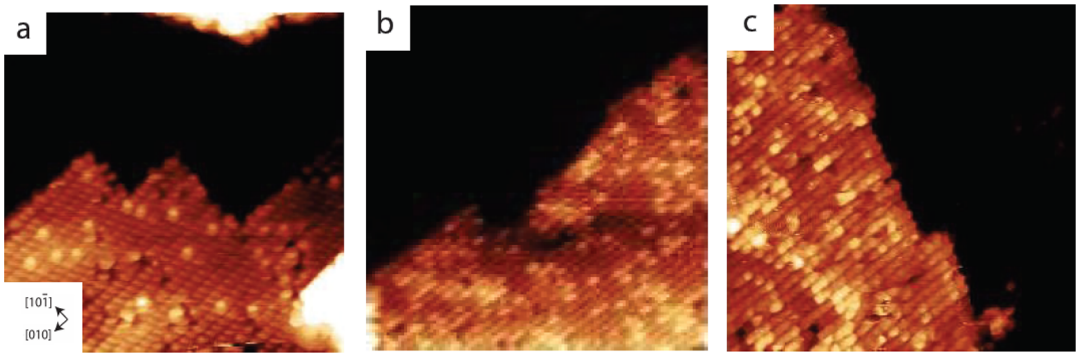

Figure 5. STM images obtained after A_{101} has been progressively electron irradiated (without surface repreparation). (a) 13 × 13 nm^2 STM image (V_s = +1.6 V, I_t = 0.5 nA) of A_{101} after electron irradiation at 500 eV, for 30 s and at a density of 37 $\mu A.cm^{-2}$. This image is identical to Figure 3a. (b) 15 × 15 nm^2 STM image (V_s = +1.6 V, I_t = 0.4 nA) after the surface in part a was electron irradiated at 500 eV, for 30 s and at a density of 74 $\mu A.cm^{-2}$. (c) 15 × 15 nm^2 STM image (V_s = +1.0 V, I_t = 0.3 nA) after the surface in part b was electron irradiated at 500 eV, for 30 s and at a density of 150 $\mu A.cm^{-2}$.

Table 2. Surface ML Coverages of the Electron Irradiated A_{101} Presented in Figure 5

electron energy (eV)	current density ($\mu A\ cm^{-2}$)	duration (s)	ML coverage
500	37	30	0.05 ± 0.01
500	74	30	0.20 ± 0.06
500	150	30	0.22 ± 0.08

interest—see Figure 5b and c—is that the bright features appear to begin to cluster. This clustering phenomenon may be associated with OH_{br} stabilization at higher coverages. V_o have been reported to form subsurface vacancy clusters,[16] presumably due to favorable energetics and stabilization.

Let us now consider other possible origins of the bright features observed in Figures 3−5. Post-electron irradiation, we do not expect to observe V_o on A_{101}. In our experiment, we operate at room temperature where the sample is heated by the filament during electron irradiation followed by at least 15 min required to transfer the sample from the electron irradiation position to tunneling conditions for STM. Subsequently, a further duration of time is necessary to obtain high resolution "atomic-resolved" STM images. Given that V_o start to move toward the bulk at temperatures as low as 200 K,[16] little or no V_o will exist on the surface with our experimental procedure. STM at 78 K of electron irradiated A_{101} shows features assigned as V_o that upon annealing for 10 min at 326 K result in what is described as subsurface oxygen vacancy clusters[16]—a phenomenon not observed in our work. This may be because heating could allow the V_o to diffuse along thermally activated pathways into the subsurface and then bulk such that it is not possible to probe with STM. Previous STM studies have investigated the adsorption of H_2O,[18,20,22] OH_t,[18,22] CO,[22,37] and O_2[18,22,38] on A_{101}. The findings are unlike the bright features observed here with a number of tips.

As single atomic defects on A_{101}, the STM appearance of OH_{br} assigned bright feature and V_o are very similar (i.e., a bright feature above a sphere-like feature), making it difficult to differentiate the two species with STM alone. In the literature, low temperature STM shows that the adsorption of diatomic species on A_{101}, such as CO, O_2, and OH_t, presents "dimer-like" features where species are differentiated effectively by their behavior.[22] Similarly, OH_{br} and V_o can be differentiated by their behavior. In our STM, at room temperature, OH_{br} has been shown to be stable on the surface, whereas V_o stability on the surface is restricted to temperatures below 200 K.[16] Above 200 K, V_o are increasingly mobile, resulting in subsurface vacancy cluster formation or V_o migration to the bulk. The temperature dependent behavior of OH_{br} and V_o can be effectively used to differentiate the two species.

Previous STM studies of electron irradiated A_{101} have been performed at 6−78 K, where V_o are observed.[16−18] In these publications,[16−18] there is no report of OH_{br} formation, which can be attributed to the low levels of residual H_2O in the respective UHV chamber (base pressure at $\times 10^{-11}$ to $\times 10^{-12}$ mbar). Alternatively, an activation barrier to water dissociation may prevent OH_{br} formation, as is the case on R_{110}.[39] At room temperature, STM[40] of electron irradiated A_{101} has been pursued to understand Au and Pt nanoparticle interaction with V_o. Postelectron irradiation STM shows some features which are similar to the bright features shown in Figures 3−5, which were tentatively assigned to V_o. However, it has since become apparent that V_o are unstable on the surface at room temperature.[16] Hence, it is reasonable to suppose that the previously observed features arise from OH_{br} species, similar to the bright features observed in our work.

4. CONCLUSION

The formation of OH species on A_{101} is a key step in H_2O dissociation. We have electron irradiated A_{101} to probe if the residual H_2O in UHV is sufficient to quench the resulting V_o and form OH_{br} groups. Our STM images show that this results in the formation of bright features on the surface, which we assign as OH_{br} species. This claim is supported by theoretical calculations[25,26] and our previously published spectroscopic measurements.[30]

AUTHOR INFORMATION

Corresponding Author

*E-mail: g.thornton@ucl.ac.uk.

ORCID

Geoff Thornton: 0000-0002-1616-5606

Notes

The authors declare no competing financial interest.

ACKNOWLEDGMENTS

We thank Yu Zhang for useful discussions. This work was supported by the European Research Council Advanced Grant ENERGYSURF to G.T., EPSRC (EP/L015862/1), EU COST

DOI: 10.1021/acs.jpcb.7b06955
J. Phys. Chem. B XXXX, XXX, XXX−XXX

action 1104 and the Royal Society through a Wolfson Research Merit Award.

REFERENCES

(1) Chen, X. B.; Shen, S. H.; Guo, L. J.; Mao, S. S. Semiconductor-Based Photocatalytic Hydrogen Generation. *Chem. Rev.* **2010**, *110*, 6503−6570.
(2) Fujishima, A.; Honda, K. Electrochemical Photolysis of Water at a Semiconductor Electroode. *Nature* **1972**, *238*, 37−38.
(3) Ni, M.; Leung, M. K. H.; Leung, D. Y. C.; Sumathy, K. A Review and Recent Developments in Photocatalytic Water-Splitting using TiO_2 for Hydrogen Production. *Renewable Sustainable Energy Rev.* **2007**, *11*, 401−425.
(4) Asahi, R.; Morikawa, T.; Irie, H.; Ohwaki, T. Nitrogen-Doped Titanium Dioxide as Visible-Light-Sensitive Photocatalyst: Designs, Developments, and Prospects. *Chem. Rev.* **2014**, *114*, 9824−9852.
(5) Hashimoto, K.; Irie, H.; Fujishima, A. TiO_2 Photocatalysis: A Historical Overview and Future Prospects. *Jpn. J. Appl. Phys. 1* **2005**, *44*, 8269−8285.
(6) Schneider, J.; Matsuoka, M.; Takeuchi, M.; Zhang, J. L.; Horiuchi, Y.; Anpo, M.; Bahnemann, D. W. Understanding TiO_2 Photocatalysis: Mechanisms and Materials. *Chem. Rev.* **2014**, *114*, 9919−9986.
(7) Zhang, H. J.; Chen, G. H.; Bahnemann, D. W. Photoelectrocatalytic Materials for Environmental Applications. *J. Mater. Chem.* **2009**, *19*, 5089−5121.
(8) Landmann, M.; Rauls, E.; Schmidt, W. G. The Electronic Structure and Optical Response of Rutile, Anatase and Brookite TiO_2. *J. Phys.: Condens. Matter* **2012**, *24*, 195503.
(9) Pang, C. L.; Lindsay, R.; Thornton, G. Chemical Reactions on Rutile TiO_2 (110). *Chem. Soc. Rev.* **2008**, *37*, 2328−2353.
(10) Pang, C. L.; Lindsay, R.; Thornton, G. Structure of Clean and Adsorbate-Covered Single-Crystal Rutile TiO_2 Surfaces. *Chem. Rev.* **2013**, *113*, 3887−3948.
(11) Diebold, U. The Surface Science of Titanium Dioxide. *Surf. Sci. Rep.* **2003**, *48*, 53−229.
(12) Thompson, T. L.; Yates, J. T. Surface Science Studies of the Photoactivation of TiO_2-New Photochemical Processes. *Chem. Rev.* **2006**, *106*, 4428−4453.
(13) Linsebigler, A. L.; Lu, G. Q.; Yates, J. T. Photocatalysis on TiO_2 Surfaces- Principles, Mechanism, and Selected Results. *Chem. Rev.* **1995**, *95*, 735−758.
(14) Hebenstreit, W.; Ruzycki, N.; Herman, G. S.; Gao, Y.; Diebold, U. Scanning Tunneling Microscopy Investigation of the TiO_2 Anatase (101) Surface. *Phys. Rev. B: Condens. Matter Mater. Phys.* **2000**, *62*, R16334−R16336.
(15) Treacy, J. P. W.; Hussain, H.; Torrelles, X.; Grinter, D. C.; Cabailh, G.; Bikondoa, O.; Nicklin, C.; Selcuk, S.; Selloni, A.; Lindsay, R.; et al. Geometric Structure of Anatase TiO_2 (101). *Phys. Rev. B: Condens. Matter Mater. Phys.* **2017**, *95*, 075416.
(16) Scheiber, P.; Fidler, M.; Dulub, O.; Schmid, M.; Diebold, U.; Hou, W. Y.; Aschauer, U.; Selloni, A. (Sub)Surface Mobility of Oxygen Vacancies at the TiO_2 Anatase (101) Surface. *Phys. Rev. Lett.* **2012**, *109*, 136103.
(17) Setvin, M.; Schmid, M.; Diebold, U. Aggregation and Electronically Induced Migration of Oxygen Vacancies in TiO_2 Anatase. *Phys. Rev. B: Condens. Matter Mater. Phys.* **2015**, *91*, 195403.
(18) Setvin, M.; Aschauer, U.; Hulva, J.; Simschitz, T.; Daniel, B.; Schmid, M.; Selloni, A.; Diebold, U. Following the Reduction of Oxygen on TiO_2 Anatase (101) Step by Step. *J. Am. Chem. Soc.* **2016**, *138*, 9565−9571.
(19) Herman, G. S.; Dohnalek, Z.; Ruzycki, N.; Diebold, U. Experimental Investigation of the Interaction of Water and Methanol with Anatase-TiO_2 (101). *J. Phys. Chem. B* **2003**, *107*, 2788−2795.
(20) He, Y. B.; Tilocca, A.; Dulub, O.; Selloni, A.; Diebold, U. Local Ordering and Electronic Signatures of Submonolayer Water on Anatase TiO_2 (101). *Nat. Mater.* **2009**, *8*, 585−589.
(21) Walle, L. E.; Borg, A.; Johansson, E. M. J.; Plogmaker, S.; Rensmo, H.; Uvdal, P.; Sandell, A. Mixed Dissociative and Molecular Water Adsorption on Anatase TiO_2 (101). *J. Phys. Chem. C* **2011**, *115*, 9545−9550.
(22) Setvin, M.; Daniel, B.; Aschauer, U.; Hou, W.; Li, Y. F.; Schmid, M.; Selloni, A.; Diebold, U. Identification of Adsorbed Molecules via STM Tip Manipulation: CO, H_2O, and O_2 on TiO_2 Anatase (101). *Phys. Chem. Chem. Phys.* **2014**, *16*, 21524−21530.
(23) Jackman, M. J.; Thomas, A. G.; Muryn, C. Photoelectron Spectroscopy Study of Stoichiometric and Reduced Anatase TiO_2 (101) Surfaces: The Effect of Subsurface Defects on Water Adsorption at Near-Ambient Pressures. *J. Phys. Chem. C* **2015**, *119*, 13682−13690.
(24) Geng, Z. H.; Chen, X.; Yang, W. S.; Guo, Q.; Xu, C. B.; Dai, D. X.; Yang, X. M. Highly Efficient Water Dissociation on Anatase TiO_2 (101). *J. Phys. Chem. C* **2016**, *120*, 26807−26813.
(25) Tilocca, A.; Selloni, A. Reaction Pathway and Free Energy Barrier for Defect-Induced Water Dissociation on the (101) Surface of TiO_2 Anatase. *J. Chem. Phys.* **2003**, *119*, 7445−7450.
(26) Tilocca, A.; Selloni, A. Structure and Reactivity of Water Layers on Defect-Free and Defective Anatase TiO_2 (101) Surfaces. *J. Phys. Chem. B* **2004**, *108*, 4743−4751.
(27) Selcuk, S.; Selloni, A. Facet-Dependent Trapping and Dynamics of Excess Electrons at Anatase TiO_2 Surfaces and Aqueous Interfaces. *Nat. Mater.* **2016**, *15*, 1107−1113.
(28) Futera, Z.; English, N. J. Exploring Rutile (110) and Anatase (101) TiO_2 Water Interfaces by Reactive Force-Field Simulations. *J. Phys. Chem. C* **2017**, *121*, 6701−6711.
(29) Stetsovych, O.; Todorovic, M.; Shimizu, T. K.; Moreno, C.; Ryan, J. W.; Leon, C. P.; Sagisaka, K.; Palomares, E.; Matolin, V.; Fujita, D.; et al. Atomic Species Identification at the (101) Anatase Surface by Simultaneous Scanning Tunnelling and Atomic Force Microscopy. *Nat. Commun.* **2015**, *6*, 7265.
(30) Payne, D. T.; Zhang, Y.; Pang, C. L.; Fielding, H. H.; Thornton, G. Creating Excess Electrons at the Anatase TiO_2 (101) Surface. *Top. Catal.* **2017**, *60*, 392−400.
(31) Setvin, M.; Daniel, B.; Mansfeldova, V.; Kavan, L.; Scheiber, P.; Fidler, M.; Schmid, M.; Diebold, U. Surface Preparation of TiO_2 Anatase (101): Pitfalls and How to Avoid Them. *Surf. Sci.* **2014**, *626*, 61−67.
(32) Setvin, M.; Franchini, C.; Hao, X. F.; Schmid, M.; Janotti, A.; Kaltak, M.; Van de Walle, C. G.; Kresse, G.; Diebold, U. Direct View at Excess Electrons in TiO_2 Rutile and Anatase. *Phys. Rev. Lett.* **2014**, *113*, 086402.
(33) Wendt, S.; Matthiesen, J.; Schaub, R.; Vestergaard, E. K.; Laegsgaard, E.; Besenbacher, F.; Hammer, B. Formation and Splitting of Paired Hydroxyl Groups on Reduced TiO_2 (110). *Phys. Rev. Lett.* **2006**, *96*, 066107.
(34) Zhang, Z.; Bondarchuk, O.; Kay, B. D.; White, J. M.; Dohnalek, Z. Imaging Water Dissociation on TiO_2 (110): Evidence for Inequivalent Geminate OH groups. *J. Phys. Chem. B* **2006**, *110*, 21840−21845.
(35) Pang, C. L.; Bikondoa, O.; Humphrey, D. S.; Papageorgiou, A. C.; Cabailh, G.; Ithnin, R.; Chen, Q.; Muryn, C. A.; Onishi, H.; Thornton, G. Tailored TiO_2 (110) Surfaces and their Reactivity. *Nanotechnology* **2006**, *17*, 5397−5405.
(36) Bikondoa, O.; Pang, C. L.; Ithnin, R.; Muryn, C. A.; Onishi, H.; Thornton, G. Direct Visualization of Defect-Mediated Dissociation of Water on TiO_2 (110). *Nat. Mater.* **2006**, *5*, 189−192.
(37) Setvin, M.; Buchholz, M.; Hou, W. Y.; Zhang, C.; Stoger, B.; Hulva, J.; Simschitz, T.; Shi, X.; Pavelec, J.; Parkinson, G. S.; et al. A Multitechnique Study of CO Adsorption on the TiO_2 Anatase (101) Surface. *J. Phys. Chem. C* **2015**, *119*, 21044−21052.
(38) Setvin, M.; Aschauer, U.; Scheiber, P.; Li, Y. F.; Hou, W. Y.; Schmid, M.; Selloni, A.; Diebold, U. Reaction of O_2 with Subsurface Oxygen Vacancies on TiO_2 Anatase (101). *Science* **2013**, *341*, 988−991.
(39) Brookes, I. M.; Muryn, C. A.; Thornton, G. Imaging Water Dissociation on TiO_2 (110). *Phys. Rev. Lett.* **2001**, *87*, 266103.
(40) Gong, X. Q.; Selloni, A.; Dulub, O.; Jacobson, P.; Diebold, U. Small Au and Pt Clusters at the Anatase TiO_2 (101) Surface: Behavior

DOI: 10.1021/acs.jpcb.7b06955
J. Phys. Chem. B XXXX, XXX, XXX−XXX

at Terraces, Steps, and Surface Oxygen Vacancies. *J. Am. Chem. Soc.* **2008**, *130*, 370−381.

DOI: 10.1021/acs.jpcb.7b06955
J. Phys. Chem. B XXXX, XXX, XXX−XXX